ChemComm

Check for updates

Optical sensor array of chiral MOF-based Fabry–Pérot films for enantioselective odor sensing†

Kuo Zhan, [ab] Yunzhe Jiang [a] and Lars Heinke (iD) *[a]

An optical sensor array based on photonic Fabry–Pérot films of surface-mounted metal–organic-frameworks (SURMOFs) with different homochiral structures is presented. It is used to detect and enantioselectively discriminant 3 pairs of chiral odor molecules, either pure or in binary mixtures.

Chirality and enantioselectivity are fundamental in nature and chiral messenger molecules are often the key to biological information transmission.[1–3] Most chiral odor molecules have an enantioselective smell, which can be typically discriminated by the human olfactory system.[4] One of the most popular examples is limonene: While the *R*-isomer of limonene (*R*-Lim) has an odor of an orange, the *S*-isomer (*S*-Lim) smells like lemons.[4] Another example is 1-phenylethanol: the *R*-isomer (*R*-PhOH) has a floral, earthy-green odor, while the odor of the *S*-isomer (*S*-PhOH) is described like a mild hyacinth with strawberry nuances.[5] For accurate discrimination, the chiral odors are mostly detected through enantioselective chromatography with homochiral columns.[6] However, due to its complexity, time-consumption and costs, it is not suited for practical sensor applications. Several efforts have been made to fabricate portable enantioselective sensors based on different chiral materials such as chiral polymers,[7] supramolecular chiral systems,[8] cyclodextrin,[9–11] carbon-nanotubes,[12] or graphene functionalized with chiral molecules.[13] For example, DNA-functionalized carbon nanotubes have been used for the distinction of *R*- and *S*-enantiomers of α-pinene as well as of β-pinene and limonene (separately).[14]

Portable enantioselective optical sensing has been demonstrated with designed fluorescence[15] and colorimetric sensors using labels, such as chiral functionalized silver nanoparticles

or Au–Ag alloy nanoparticles.[16,17] However, due to the strong intermolecular interactions between the sensor labels and the analytes, these label-based sensors operate typically not in a reversible and repeatable manner. Optical, label-free sensors that detect and discriminate the enantiomers of various molecules (even in their pure form) have not yet been presented.

A Fabry–Pérot (FP) cavity is an interferometric optical structure, constructed by a thin film in between two reflectors. The photonic properties of the FP-film are controlled by the thickness and reflective index (RI) of the inner film, see ESI.†[18] Based on this, FP-films have been widely used as optical chemical sensors.[18,19] Using the changes of the reflection spectrum caused by the uptake of guest molecules as sensor signal, FP-sensors can detect the targeted analytes accurately and conveniently. To make optical sensors based on FP-films, transparent and porous materials are required. Thin films of metal–organic frameworks (MOFs) seem ideally suited for such tasks.[20,21] MOFs consist of metal nodes connected by organic ligand molecules, forming a regular porous scaffold. MOFs possess many unique properties, such as high specific surface areas, very diversified structures and tailorable functionalities.[22] All these properties are favorable for applications in sensors. For FP-based sensing, the MOF materials need to be prepared in the form of thin films. There, the layer-by-layer synthesis seems ideally suited, resulting in surface-mounted MOF (SURMOF) films which have typically a homogeneous morphology with a high degree of structural order and a low defect density.[23] In a previous study, a gravimetric sensor array based on homochiral and achiral SURMOFs was used to discriminate the enantiomers of 5 pairs of chiral odors simultaneously.[24] Optical sensors based on chiral MOF films have not yet been presented.

Here, we present a label-free optical sensor array based on homochiral and achiral FP-SURMOF films. The sensor array is made of SURMOFs with different structures, which are Cu-based homochiral MOFs (Cu$_2$(DCam)$_2$(dabco)[25] and Cu$_2$-(DCam)$_2$(Bipy))[25] and achiral HKUST-1.[26,27] (DCam stands for chiral (*1R,3S*)-(+)-camphoric acid as layer linker, dabco for

[a] Karlsruhe Institute of Technology (KIT), Institute of Functional Interfaces (IFG), Eggenstein Leopoldshafen 76344, Germany. E-mail: Lars.Heinke@kit.edu
[b] Beijing Jiaotong University (BJTU), School of Physical Science and Engineering, Beijing 100044, China

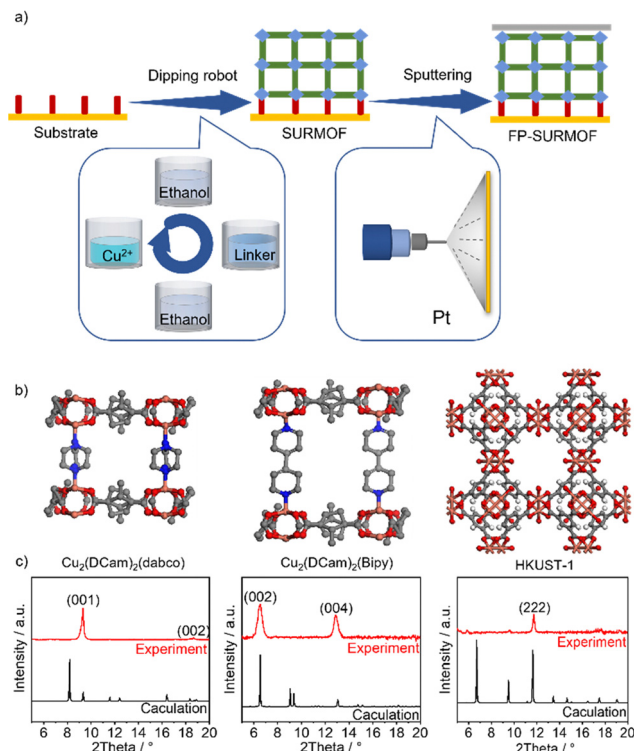† Electronic supplementary information (ESI) available. See DOI: https://doi.org/10.1039/d3cc01298k

This journal is © The Royal Society of Chemistry 2023

Fig. 1 (a) The synthesis of the FP-chiral-SURMOF films. (b) Sketches of the SURMOF structures, which are $Cu_2(DCam)_2(dabco)$, $Cu_2(DCam)_2(Bipy)$, HKUST-1, left to right, see labels. (c) X-ray diffractograms of the SURMOFs, see labels. The X-ray wavelength is 0.154 nm.

1,4-diazabicyclo[2.2.2]octane and BiPy for 4,4′-bipyridine as pillar linkers, HKUST-1 stands for Hong Kong University of Science and Technology 1.) Based on the three SURMOFs, we prepared a FP-chiral-SURMOF sensor array. The sensor array in combination with UV-vis spectroscopy is able to reversibly detect 3 pairs of different chiral odors at low concentrations with limits of detection (LODs) in the order of 10–40 ppm. Using simple machine learning algorithms to analyze the data, the sensor array can enantioselectively distinguish all six isomers at 100 ppm with a very high classification accuracy of 98.6%. Furthermore, the FP-chiral-SURMOF sensor array is also successfully applied to precisely discriminate the R-/S-Lim binary mixture odors in different ratios. We also demonstrate that the sensor read-out can be performed with the digital camera of a common smart phone, avoiding expensive lab equipment.

The SURMOF films with different structures were prepared in a layer-by-layer fashion,[23] as outlined in Fig. 1a. The substrates, which are 11-mercapto-1-undecanol-functionalized gold-coated silicon wafer, were alternatively immersed in the ethanolic solutions of the metal nodes and of the linker molecules, see SI. The metal nodes are copper acetate. The linker molecules are DCam and dabco for $Cu_2(DCam)_2(dabco)$, DCam and Bipy for $Cu_2(DCam)_2(Bipy)$ and trimesic acid (BTC) for HKUST-1 (see Fig. 1b). The syntheses were performed with a dipping robot with 180 cycles each.[25] To enhance the SURMOF quality and to decrease the surface roughness, ultrasonication was used to improve the cleaning process.[28] On top of the chiral

SURMOF films, platinum films of about 5 nm thickness were sputtered. The Pt film acts as a mirror, resulting in the FP-SURMOF films. The crystallinity of the SURMOF films was explored by X-ray diffraction (XRD), showing that the films have a crystalline structure which correspond to the targeted MOF structures, Fig. 1c. The diffractograms after all sensing experiments are essentially identical to the diffractograms of the pristine samples, Fig. S14 (ESI†), indicating the stability of the SURMOFs. The samples were further characterized by infrared reflection absorption spectroscopy (IRRAS, Fig. S1, ESI†), verifying the composition of the SURMOFs. The cross-section SEM images, Fig. S2 (ESI†), show that the SURMOF films have a homogeneous morphology. The film thicknesses of all SURMOFs are approximately 500 nm.

The sensing performance of the FP-chiral-SURMOFs sensor array was tested with 3 pairs of chiral odors as analytes. The analytes are R- and S-1-phenylethylamine (R-PEA, S-PEA), R- and S-1-phenylethanol (R-PhOH, S-PhOH) and R- and S-Limonene (R-Lim, S-Lim), see Table S2, ESI.† The UV-vis spectra of the FP-chiral-SURMOF films in a controlled vapor atmosphere were recorded in reflection. The reflectance spectra of the FP-$Cu_2(DCam)_2(dabco)$, FP-$Cu_2(DCam)_2(Bipy)$ and FP-HKUST-1 films, either empty (pristine) or exposed to the vapors of the chiral molecules are shown in Fig. 2a, Fig. S5 and S7 (ESI†), respectively. The spectra show a characteristic photonic reflectance
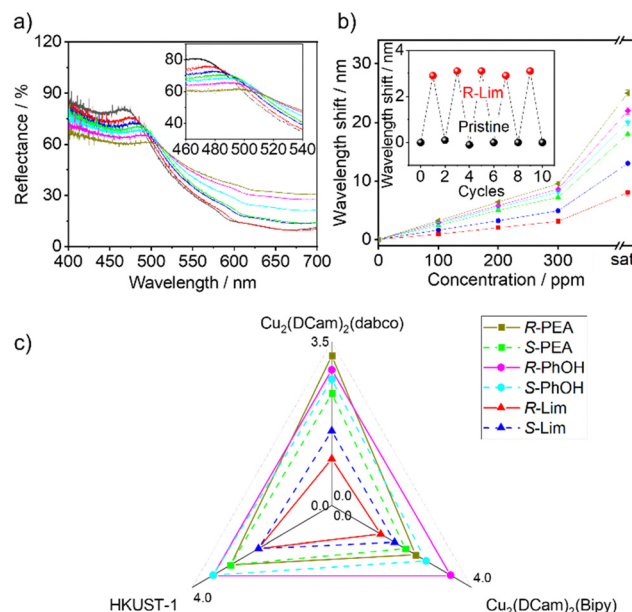

Fig. 2 (a) The reflectance spectra of the FP-$Cu_2(DCam)_2(dabco)$ film in the atmosphere of the saturated analytes, see labels in (c). The same color code is used in all panels. (b) The wavelength shift of the reflectance peak of the FP-$Cu_2(DCam)_2(dabco)$ film in different analyte vapors *versus* concentration. The UV-vis reflectance spectra for the FP-$Cu_2(DCam)_2(Bipy)$ and FP-HKUST-1 films are shown in Fig. S4–S9 (ESI†). The inset shows the wavelength shift of the reflectance peak of the FP-$Cu_2(DCam)_2(dabco)$ film for 300 ppm R-Lim, testing the repeatability and reproducibility. (c) Radar plot of the wavelength-sensitivity (see slope in b) in the range of 0–300 ppm) in the sensors. The units of the axes are 10^{-2} nm ppm^{-1}.

peak (at 466 nm for $Cu_2(DCam)_2(dabco)$, 462 nm for $Cu_2(DCam)_2$-(Bipy) and 578 nm for HKUST-1). These peaks shift to larger wavelengths and their intensities decrease upon analyte exposure, see also SI. This is caused by the increase of the reflective index of the SURMOF when the analyte molecules are adsorbed in the pores. The reflectance-peak wavelength shifts linearly with the analyte concentration for all analytes in the considered concentration range (0–300ppm), Fig. 2b. The slopes in this plot are regarded as the sensitivity. This allows the calculation of the limits of detection (LODs), Table S2, ESI.† Since the sensitivity and LOD are based on the wavelength shift of the photonic peak, we refer to them as wavelength-sensitivity and wavelength-LOD.

In addition to the wavelength shift, the intensity of the photonic reflectance peak changes. The sensitivity (see Fig. S5c, ESI†) and the so calculated LOD are referred to as intensity-sensitivity and intensity-LOD, see Table S2, ESI.†

In both methods, the LODs of the sensors are in the range between 8.8 ppm and 42.9 ppm, significantly smaller than 100 ppm. (This is in line with the very high classification accuracy of the different chiral odors at 100 ppm, see below.) A closer look shows that the method based on the wavelength results in somewhat smaller LODs than the intensity method.

The repeatability is explored by repeating the 300ppm R-Lim vapor exposure, Fig. 2b inset. The data show that the sensor exposure is fully reversible and repeatable, as a result of the reversible R-Lim uptake by and release from the FP-SURMOF film.

Each FP-chiral-SURMOF sensor possesses a different sensitivity for the same analyte. Moreover, different analytes exhibit different sensitivities in the same sensor. (See Table S2 (ESI†) or the slopes in Fig. 2b, Fig. S5b and S7b (ESI†), summarized also in the radar plot Fig. 2c.) This means each analyte has a characteristic signal pattern in the sensor array, which is also shown in the characteristic fingerprint in the radar plot. This pattern allows the qualitative discrimination of the (chiral) analytes.

For determining the accuracy of the sensor array to discriminate the chiral odors, we analyzed the data with simple machine learning algorithms. In this work, we apply 3 classification machine learning algorithms which are k-Nearest Neighbor (k-NN), Support Vector Machine (SVM) and Artificial Neural Network (ANN) to identify the analytes, see ESI† and ref. 29, 30. The accuracies of the data classification are shown in the confusion matrix, Fig. 3. Fig. 3a shows the quantitative discriminations of the 3 pairs of the chiral odors at 100 ppm by ANN, indicating a correct identification with an average classification accuracy of 98.6%. Confusion matrices by the kNN and SVM analyses as well as from other concentrations (200 ppm, 300 ppm) are shown in Fig. S9–S11 (ESI†). All results show very high classification accuracies, demonstrating the sensor array of FP-chiral-SURMOF films allows the enantioselective classification of the 6 chiral odors.

The discrimination property of the sensor array toward mixtures of chiral odors was investigated by exposing the sensor array to pure R- and S-Lim as well as their binary mixtures (3:1, 1:1 and 1:3), Fig. 3b. The confusion matrix indicates a correct identification of the mixtures with an
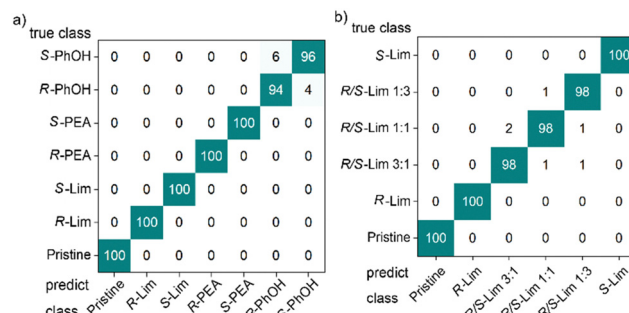

Fig. 3 (a) The ANN confusion matrix of the 3 pairs of chiral odors at a concentration of 100 ppm and the pristine (empty) sensors. (b) The ANN confusion matrix of R- and S-Lim pure (100%) and their binary mixtures (3:1, 1:1, 1:3) and the pristine (empty) sensors. The total concentration (R + S) is always 300 ppm. The true class are the rows and the predicted class are the columns. Correct classifications are shown on the main diagonal of the matrix; misclassifications are the other values.

average classification accuracy of 99%. The radar plot of the reflectance intensity change and its corresponding reflectance spectra are shown in Fig. S12 (ESI†). All the above results show that the FP-chiral-SURMOF sensor array can identify the chiral odors and also their mixtures precisely.

Based on the strong performance of the sensor array to detect and classify the chiral analytes by using its UV-vis spectra, we explore whether the sensor read-out can be performed with simple equipment. To this end, we placed the three FP-SURMOFs next to each other in a cell with controlled analyte concentration and took pictures with the digital camera of a common smart phone, Fig. 4a. From the pictures, the colors were quantified by their RGB values (Table S1, ESI†) and their positions on the CIE-color-space-map are shown in Fig. 4b. By applying simple machine-learning algorithms, the sensor response can be clearly distinguished with an average classification accuracy of 97%. This demonstrates that a simple device (here the smart-phone-camera) can be used for the sensor read out as well, avoiding lab equipment.

Summarized, we developed an optical sensor array based on FP films made of nanoporous chiral surface-mounted MOF films. This FP-chiral-SURMOF sensor array is a label-free, inexpensive and reversible sensor system. Here, the sensors are based on homochiral and achiral SURMOFs, which are $Cu_2(DCam)_2(dabco)$, $Cu_2(DCam)_2(Bipy)$ and HKUST-1. The sensor responses are obtained from their UV-vis spectra. The sensors show high sensitivities and low LODs in the range of ∼10–40 ppm for 3 pairs of chiral odors, which are R-/S-limonene, R-/S-1-phenylethanol and R-/S-1-phenylethylamine. In addition, the sensing results are fully repeatable and reversible. The analysis of the sensor-array data by simple machine learning algorithms like ANN results in a classification accuracy of 98.6% for the enantioselective discrimination of the 3 pairs of chiral odors at a concentration of 100 ppm. Moreover, different binary mixtures of R- and S-limonene could also be discriminated very precisely. We also demonstrate that the sensor read out can be performed with the camera of a common smart phone, avoiding expensive lab equipment.
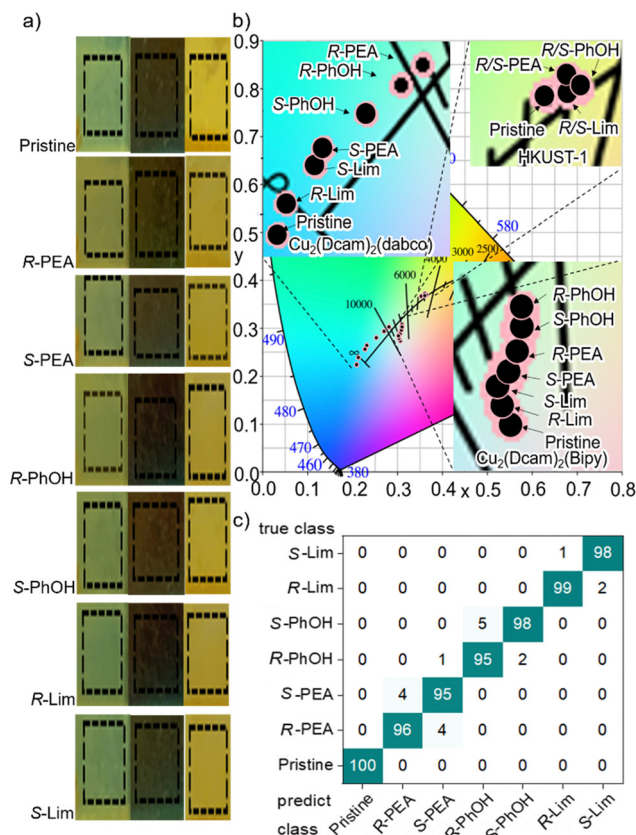
Fig. 4 (a) The FP-SURMOF sensors (left: Cu$_2$(DCam)$_2$(dabco), center: Cu$_2$(DCam)$_2$(Bipy) and right: HKUST-1) in an atmosphere of the different analytes, see labels. The dotted squares are the areas where the color (*i.e.* the RGB values, see Table S1, ESI†) were determined. (b) The sensors on the CIE-color-space map. (c) The confusion matrix to classify the chiral odors, calculated by ANN.

This work shows an inexpensive platform of very small, portable and label-free optical sensors that allows the enantio-selective discrimination of chiral odors. We foresee that various chiral SURMOF structures can be used in such FP-based sensor arrays for advanced chiral odor and vapor sensing.

Conflicts of interest

The authors declare no conflict of interest.

Notes and references

1 L. D. Barron, *Space Sci. Rev.*, 2008, **135**, 187–201.
2 A. Salam, *J. Mol. Evol.*, 1991, **33**, 105–113.
3 L. A. Nguyen, H. He and C. Pham-Huy, *Int. J. Biomed. Sci.*, 2006, **2**, 85.
4 R. Bentley, *Chem. Rev.*, 2006, **106**, 4099–4112.
5 G. C. Kite and W. L. Hetterscheid, *Phytochemistry*, 2017, **142**, 126–142.
6 A. Berthod, *Chiral recognition in separation methods*, Springer, 2010.
7 L. Torsi, G. Farinola, F. Marinelli, M. Tanese and O. Omar, *Nat. Mater.*, 2008, **7**, 412–417.
8 G. A. Hembury, V. V. Borovkov and Y. Inoue, *Chem. Rev.*, 2008, **108**, 1–73.
9 C. Fietzek, T. Hermle, W. Rosenstiel and V. Schurig, *Fresenius' J. Anal. Chem.*, 2001, **371**, 58–63.
10 K. Bodenhöfer, A. Hierlemann, M. Juza, V. Schurig and W. Göpel, *Anal. Chem.*, 1997, **69**, 4017–4031.
11 P. Kurzawski, V. Schurig and A. Hierlemann, *Anal. Chem.*, 2009, **81**, 9353–9364.
12 N. J. Kybert, M. B. Lerner, J. S. Yodh, G. Preti and A. C. Johnson, *ACS Nano*, 2013, **7**, 2800–2807.
13 Y. Zhang, X. Liu, S. Qiu, Q. Zhang, W. Tang, H. Liu, Y. Guo, Y. Ma, X. Guo and Y. Liu, *J. Am. Chem. Soc.*, 2019, **141**, 14643–14649.
14 K. Wen, S. Yu, Z. Huang, L. Chen, M. Xiao, X. Yu and L. Pu, *J. Am. Chem. Soc.*, 2015, **137**, 4517–4524.
15 E. Zor, *Talanta*, 2018, **184**, 149–155.
16 J. Wei, Y. Guo, J. Li, M. Yuan, T. Long and Z. Liu, *Anal. Chem.*, 2017, **89**, 9781–9787.
17 M. Y. Mulla, E. Tuccori, M. Magliulo, G. Lattanzi, G. Palazzo, K. Persaud and L. Torsi, *Nat. Commun.*, 2015, **6**, 6010.
18 M. R. Islam, M. M. Ali, M.-H. Lai, K.-S. Lim and H. Ahmad, *Sensors*, 2014, **14**, 7451–7488.
19 J. Buchmann, E. Zhang, C. Scharfenorth, B. Spannekrebs, C. Villringer and J. Laufer, *Evaluation of Fabry-Perot polymer film sensors made using hard dielectric mirror deposition*, SPIE, 2016.
20 I. Stassen, N. Burtch, A. Talin, P. Falcaro, M. Allendorf and R. Ameloot, *Chem. Soc. Rev.*, 2017, **46**, 3185–3241.
21 P. Falcaro, R. Ricco, C. M. Doherty, K. Liang, A. J. Hill and M. J. Styles, *Chem. Soc. Rev.*, 2014, **43**, 5513–5560.
22 S. Kitagawa, *Chem. Soc. Rev.*, 2014, **43**, 5415–5418.
23 L. Heinke and C. Wöll, *Adv. Mater.*, 2019, **31**, 1806324.
24 S. Okur, P. Qin, A. Chandresh, C. Li, Z. Zhang, U. Lemmer and L. Heinke, *Angew. Chem., Int. Ed.*, 2021, **60**, 3566–3571.
25 Z.-G. Gu, S. Grosjean, S. Bräse, C. Wöll and L. Heinke, *Chem. Commun.*, 2015, **51**, 8998–9001.
26 S. S. Y. Chui, S. M. F. Lo, J. P. H. Charmant, A. G. Orpen and I. D. Williams, *Science*, 1999, **283**, 1148–1150.
27 K. Müller, J. S. Malhi, J. Wohlgemuth, R. A. Fischer, C. Wöll, H. Gliemann and L. Heinke, *Dalton Trans.*, 2018, **47**, 16474–16479.
28 Z. Gu, *Microporous Mesoporous Mater.*, 2015, **211**, 82–87.
29 P. Qin, B. A. Day, S. Okur, C. Li, A. Chandresh, C. E. Wilmer and L. Heinke, *ACS Sens.*, 2022, **7**, 1666–1675.
30 P. Qin, S. Okur, C. Li, A. Chandresh, D. Mutruc, S. Hecht and L. Heinke, *Chem. Sci.*, 2021, **12**, 15700–15709.